

# Aerodynamic Performance Study of a Modern Blended-Wing-Body Aircraft Under Severe Weather Situations

Tung Wan<sup>1</sup> and Bo-Chang Song<sup>2</sup>

*Department of Aerospace Engineering, Tamkang University, Tamsui, Taipei, 251, Taiwan, Republic of China*

Due to the high fuel cost in recent years, more efficient flight vehicle configurations are urgently needed. Studies have shown remarkable performance improvements for the Blended-Wing-Body (BWB) over conventional subsonic transport. Also, aircraft during taking-off and landing might face strong crosswind and heavy rain, and these effects may be even more detrimental for BWB due to its peculiar configuration. In this study, a 3-D BWB is first constructed and numerically validated, and heavy rain effects are simulated mainly through two-phase flow approach. Three crosswinds considered are 10m/s, 20m/s and 30m/s, and the resulting BWB's low speed stability derivative values under crosswind are different from typical transport, representing the intrinsic nature of BWB static unstable tendency. Also, the heavy rain influence to BWB is that lift decrease and drag increase at all angle of attack spectra, and liquid water content of 39g/m<sup>3</sup> is more detrimental than 25g/m<sup>3</sup>, with maximum reduction of lift at 0 degree and maximum increase of drag at 6 degree angle of attack during taking-off and landing. The degradation in maximum lift to drag ratio could reach a stunning 10 to 15 percent at low angle of attack attitude.

## Nomenclature

$C_L$	Lift coefficient
$C_D$	Drag coefficient
$C_l$	Rolling-moment coefficient
$C_m$	Pitching-moment coefficient
$C_n$	Yawing-moment coefficient
$\alpha$	Angle of attack, deg
$\beta$	Side-slip angle, deg
L/D	Lift to Drag Ratio
$d_p$	Droplet particle diameter
$R_e$	Reynolds number

## I. Introduction

IN order to cost down operation expenses in a highly competitive market environment, aviation industry always demand for more efficient aircrafts. To cope with high passenger demand also requires new aircraft configurations to improve operational efficiency, productivity and customer satisfaction. Thus subsonic performance design of conventional large transport aircraft is in light of this to revolutionize their aircraft shape. One of the non-conventional aircraft design concepts was proposed early as flying wing; later evolves to become the Blended-Wing-Body (BWB) aircraft. BWB has a no tail design shape, and it is an integration of fuselage and wing. Compared with the traditional tube-and-wing shape, its aircraft performance enhancement has long being recognized. BWB would be a tremendous technology research and an important goal of development, and clearly it shows significant advantage over conventional aircraft in terms of performance and weight. Generally speaking, the main aerodynamic advantage of the BWB is its lift to drag ratio can increase as much as 20% than conventional aircraft,

---

<sup>1</sup> Associate Professor, Department of Aerospace Engineering, 151 Ying-chuan Road, Tamsui, Taipei, Taiwan, Republic of China, AIAA member.

<sup>2</sup> Graduate Student, Department of Aerospace Engineering, 151 Ying-chuan Road, Tamsui, Taipei, Taiwan, Republic of China.

and nowadays the aircrafts must comply with more strict environmental requirements, it seems to be the optimized transport aircraft in the future.

But a review of aircraft accident records in the past decades shows the necessity of aircraft avoiding the most severe weather environments. As pointed out by Wan and Wu,<sup>1</sup> the adverse weather can be a hazardous factor to aircraft flight, especially during take-off and landing phases. Among numerous weather factors that influence the aircraft during take-off and landing, most serious factors are crosswind, low level wind shear, ice accretion, heavy rain, etc. More often, we do not have enough time to take precaution action since flight incident happened so quickly, thus we shall pay more attention to the environment that can influence aircraft performance during the take-off and landing phases.

Airplane fly through heavy rain has been postulated as cause in several weather conditions associated with aerodynamic penalty. Even today, with modern weather radar on board to improve weather forecasting, heavy rain rates above 1000 mm/hr can still significantly affect performance of commercial aircraft, say lift decrease up to 30% and drag increase up to 20%. On the other hand, BWB vehicle lacks the typical control surfaces as in the conventional aircraft, such as rudder and elevator in a separate tail. But it is still important for civil aircraft to be statically stable in flight, thus the BWB lateral stability performance under crosswind will become the second focus of our consideration. This paper represents the outcome of a series of our BWB works, and current goal is to investigate the feasibility of CFD tool Fluent<sup>2</sup> on BWB aerodynamic performance and stability degradation behavior under severe weather such as heavy rain and cross winds.

## II. Research Background

Unconventional aircraft configurations such as BWB are being evolved from flying wing designs, and defined as having the wing and fuselage blending together and resembles flying wing shape. The flying wing configuration is not new; in 1929 the Junkers G.38 was the largest airplane in the world at that time;<sup>3</sup> wingspan measured 44 m in length and has a maximum speed of 185 km/h. This design was developed leading up to World War II, later in 1944, AW-52 was designed by Lloyd<sup>4</sup> and proposed to be a flying wing bomber with a span of 120 ft. Problems were encountered with the laminar wings and the pitch axis control problems at high speed eventually lead to its abandon in 1954. Also in 1940s, Northrop<sup>5</sup> developed a jet propelled flying wing bomber, YB-49. Small fins were added for stability at the trailing edges, but still in 1948 it was found that the YB-49 was extremely unstable and very difficult to fly. This stagnation of flying wing design was finally broken in the 80s, NASA developed and improved advanced subsonic BWB transports, in particular airplane for very large transport that are more efficient and environmentally friendly. In 1988, The B-2 Spirit was publicly displayed,<sup>6</sup> and due to the merge of fuselage and wing, it has better lift to drag ratio. The revolutionary amalgamation of low-observable characteristics with high aerodynamic efficiency and large payload gives the B-2 advantages over existing bombers.

Then in 1998, Liebeck et al.<sup>7</sup> introduced the concept of blends the wing, fuselage, and the engines into a single lifting surface. The biggest improvement is in aerodynamic efficiency, which has reduced surface area and thereby reduced skin friction drag. According to Liebeck's design, it is possible to achieve up to 33% reduction in surface area, representing a potential revolution in subsonic transport efficiency. In his article BWB considered to have an 800 passenger capacity, cruising at Mach 0.85 and a 7000 nm range. He also indicated for BWB a typical shock is evident on the outboard wing and becomes very weak on the center body. Behind the shock the region is suitable for engine installation. Alternatively, the center body with its large chord requires a much lower sectional lift coefficient to maintain an elliptic span load. Reduced sectional lift demand on the center body allows large thickness to maximize payload volume, without demanding a high compressibility drag penalty. Later Leifur et al.<sup>8</sup> compared the Boeing BWB-450 with the Airbus A380-700: the most noticeable result is the BWB 32% lower fuel burn per seat. Both airplanes are using equivalent engines of similar thrusts, but the A380 needs four and the BWB only three, thus BWB shows significant advantage over conventional aircraft in terms of performance and weight.

In 2002, Qin, et al.<sup>9</sup> presented the main aerodynamic advantages of the new BWB design are its lower wetted area to volume ratio and lower interference drag as compared to the conventional aircraft. Indeed, an increase in lift to drag maximum of about 20% over the conventional design has been estimated for the BWB. At the design transonic cruise and lift condition for his BWB, wave drag is a significant component of the total drag. Therefore the span loading distribution that giving minimum induced drag does not necessarily produce minimum total aerodynamic drag. In 2003, Roman et al.<sup>10</sup> studied aerodynamics of high subsonic BWB configurations, concluded that Mach number 0.93 has penalty performance relative to Mach number 0.85. Later in 2004, Qin et al.<sup>11</sup> again calculated the aerodynamic performance of BWB aircraft; they carried out 3-D aerodynamic surface optimization of

different BWB configurations and improved aerodynamic performance at cruise condition. In this study, BWB geometry built up is close to his optimized shape.

In 2009, Wan et al.<sup>12</sup> presented aerodynamic performance investigation of BWB and the influence of heavy rain condition. They achieved the optimized lift to drag ratio both at 0.85 cruise and landing conditions. The best cruise angle of attack (AOA) is found to be at 2 degree, and at landing Reynolds number of  $6.0 \times 10^7$ , the heavy rain effect on their BWB lift to drag ratio is that a maximum of 1.60 decreases or close to 10% decrease at 4 degree AOA. On the other hand, in recent years CFD tool has been used extensively in the investigation of flight vehicle dynamics.<sup>13,14</sup> For a typical six degree-of-freedom (6-DOF) aircraft motion simulation, as might be used for handling quality assessment, body-axis aerodynamic forces and moments are modeled using Taylor series expansions based on force and moment coefficients. Accurate evaluation of these force and moment coefficients magnitudes their trends are critical. Data at high AOA, side slip angle, or high angular rates may be required to model some extreme conditions. This approach is further justified for a BWB configuration recently,<sup>15</sup> and the similar concept is implemented in the current work.

In contrast, weather has always been a major threat in aviation safety. Even today, with modern weather radar aboard commercial aircraft to improve weather forecasting, it remains a foremost cause of aircraft accidents. The aerodynamics associated with aircraft fly through crosswind and heavy rain recently has been postulated to be a contributing cause in the accidents' chain of event. Thus we need to concentrate on the physics of severe weather to flight. In 1941, the earliest analytical work by Rhode et al.<sup>16</sup> indicated a DC-3 aircraft flying at 5000ft encountering a rain with liquid water content (LWC) of  $50 \text{ g/m}^3$  will associate with drag increase. He also found that decrease lift and increase drag during takeoff and landing with heavy rain would be significant. In 1976, Markowitz<sup>17</sup> established the terminal velocity of raindrops. Heavy rain droplets impact an airplane at an angle from the horizontal at a less 10 degree, and the relationship is according to raindrops size and altitude. In 1983, Haines et al.<sup>18</sup> consider the importance of heavy rain to a landing airplane. Rain can affect an airplane in at less four ways: 1. Rain drops striking the airplane convey a downward and backward momentum. 2. A thin water film results from the rain will increase the airplane mass. 3. The water film can be roughened by drop impacts and surface stresses producing aerodynamic lift and drag penalties. 4. Depending on airplane orientation, raindrops strike the airplane unevenly and thus imparting a pitching moment.

In 1987, Bilanin<sup>19</sup> indicated that under the most serve rainfalls recorded, rain rates have never exceeded 1874 mm/hr with a LWC of  $80 \text{ g/m}^3$ , but still the volume fraction occupied by water and the water-air mixture are quite dilute. For accentuate the raindrop diameter, spectrum have been measured to be in the range 0.1-6.0 mm, with 4.0 mm is the average diameter of heavy rain. Mean distance between raindrops corresponding to heavy rain is about 7 cm. In 1989, Bezos et al.<sup>20</sup> conducted rain effect sensitivity of airfoil geometry on an NACA64210 airfoil. The experimental results indicated that the rain caused premature transition from a laminar to a turbulent boundary layer. Both the heavy rain laminar and turbulent flow on NACA 64210 airfoils will experience significant decrease in maximum lift and increase drag with increasing LWC. The landing configuration was more sensitive to the rain environment, and experienced a 22% reduction in maximum lift at 8 degree AOA, decreasing the stall angle at the highest LWC of  $46 \text{ g/m}^3$ .

In 1995, Valentine et al.<sup>21</sup> implementing Lagrangian particle tracking algorithm for a thin layer Navier-Stokes code. They also established the rain splash back model, and droplets are tracked through the 2-D incompressible airflow fields around a NACA 64-210 airfoil section. Their lift and drag results are surprisingly close to the Bezos' field tests data, may be too close. Also in 1995, Thompson et al.<sup>22</sup> illustrated the complex regions of heavy rain droplets on plate surface: 1. Droplet-Impact Region: rain droplets impact on surface will form water film, and cause smaller droplets scatter back into the boundary layer flow; thus drain energy. This loss of energy leads to loss of lift and early flow separation. 2. Film-Convection Region: surface water is dragged downstream by friction, and surface waves of convection will cause smooth laminar film change into turbulence. This will lead to reductions in lift and rise in drag. 3. Rivulet-Formation Region: water film separated to rivulets and beads. Different flow rate will cause rivulet to different sinuosity, wavelength, and amplitude of the waves. 4. Droplet-Convection Region: the meandering rivulets are no longer stable and the beads slide slowly dragged by the airflow and coalescing with other beads. Momentum transfer in this region is dominated by the trailing edge flow structure. Only recently the numerical simulation of heavy rain is picked up by Wan et al.<sup>1,23</sup>, using first add droplet mass and momentum to the flow, then the two-phase flow approach to simulate NACA64210 airfoil rain effects and compared with Bezos<sup>20</sup> experimental data. The no rain situation is first validated with NACA and Bezos's experimental data, and for LWC  $25 \text{ g/m}^3$  and  $39 \text{ g/m}^3$  heavy rain cases, the tendency of lift decrease and drag increase at different AOA is created and justified. Indeed this phenomenon might get worse for BWB's large flat surface and is the focus of our work.

### III. Numerical Modeling

In this work our BWB geometry is similar to baseline geometry model;<sup>11</sup> and the configuration has been through aerodynamic optimization. The 3-D geometry as shown in Fig. 2, our BWB consists of center body and inner, outer wing; with half-span length of 38.75 m. Winglet shape is a linear interpolation of NACA 0012 airfoil joining at outlet wing-tip. The airfoil thickness distribution at different span location is approximate 17% in the center body, and reach to maximum of 18% at 6 m span location. Twist distribution of the airfoil/wing profile is that near center body and outer wing it twisted downward, and at the inner wing it twists upward, Fig. 3 is the twist angle distribution of the airfoil/wing. Leading edge sweep angle is 63.8 degree for center body and 38 degree for outer wing. Our BWB projected a shadow area of 1512.48 m<sup>2</sup> for reference area consideration, with a 34.1735 m mean aerodynamic chord length.

In this work, grids are generated through both the structured and unstructured multi-block method to ensure the grid quality. BWB has a complicated 3-D shape; after testing the mesh of 3.2, 3.6, 3.9, 4.36 million unstructured grids, we found the 4.36 million grids case achieves best L/D ratio. As for structured mesh, 32 blocks C-type grid can help us to control the skewness and number of grid cells. After the 4.1, 5.3, and 6.4 million structured grid cases tested, the 5.3 million grids can control skewness range not over 0.5 with Y plus range 250 to 400 at 0.85 Mach cruise condition. Fig. 4 shows the BWB structured near mesh for that case. Finally the 6.4 million structured mesh is chosen since it can further enhance the L/D ratio and achieve the minimum Y plus value of 6 to 16 at free stream velocity 49.4774 m/s condition, as shown in Fig. 5.

Besides the grid system, proper selection of the governing equations, boundary conditions handling, and solver scheme treatment are all vital to the convergence and accuracy of our solution. In our investigation, FLUENT is used to solve conservation equations of mass, momentum and energy in their finite volume method. Two different finite volume solvers were provided: pressure-based solver and density based solver; and two algorithms are also available: segregated and coupled algorithm. 0.85 Mach cruise condition and low speed landing condition (V=49.4774 m/s) are treated differently. In the segregated algorithm, the individual equations are solved one after another and convergence is relatively slow. Still, it is the method that most suitable for our two-phase flow computation. Thus, the 3-D segregated finite volume solver is chosen with the usual ideal gas assumption. The pressure gradient term is discretized by PRESTO (Pressure Staggering Option) method, convection term is discretized through first order upwind scheme, and the coupling of pressure of velocity is handled by the SIMPLE (Semi-implicit Method for Pressure-linked Equations) scheme in order to accelerate the converge speed.

For our simulations at Reynolds numbers  $3.0 \times 10^6$  for low speed landing and  $6.0 \times 10^7$  for cruise, the flow behaviors are characterized as turbulent, thus adding turbulence model to governing equation is an important part of our simulation. The Reynolds-averaged Navier-Stokes (RANS) equations represent transport equations for the mean flow only; with all turbulent scales have been modeled. This approach of permitting a solution for mean flow variables greatly reduces the computational effort.<sup>24</sup> With the Boussinesq hypothesis, this Reynolds-averaged approach is adopted for many engineering problems, and the Spalart-Allmaras (S-A) and  $\kappa$ - $\epsilon$  models are chosen as our turbulence model candidates, both are quite common turbulence models in use. In order to achieve the best results the S-A model is used in the M6 wing and BWB cruise conditions, while the  $\kappa$ - $\epsilon$  model is implemented in the BWB landing situation in this work.

FLUENT can simulate a discrete second phase in a Lagrangian reference frame and is called Discrete Phase Model (DPM).<sup>2</sup> The second phase consists of spherical particles to represent droplets dispersed in the continuous phase. DPM particles can model the wall-film; it allows a single component liquid droplet to impact on surface and form thin film. This DPM model can be separated into four sub-models: interaction during the initial impact with a wall boundary, subsequent tracking on surfaces, calculation of film variables, and coupling to the gas phase. The momentum transfer from the continuous phase to the discrete phase is computed by examining the change in momentum of a particle as it passes through each control volume in the model. This momentum change is computed as

$$\mathbf{F} = \sum \left( \frac{18\mu C_D R_g}{24\rho_p d_p^2} (\mathbf{u}_p - \mathbf{u}) + \mathbf{F}_{\text{other}} \right) m_p \Delta t \quad (1)$$

where  $d$  is diameter,  $\mathbf{F}_{\text{other}}$  is other interaction force per unit mass, and subscript  $p$  stands for droplet particle.

For DPM input parameters, we need to input the particle diameter, velocity and mass flow rate for every injection point. As pointed out in our previous work, we can set particle diameter as 4 mm and each particle distance is 7 cm. Particle velocity is the droplet terminal velocity 8.81 m/s which is function of droplet diameter.<sup>17</sup> The

injection plane is  $60.2 \times 10.01$  m, and the rain mass flow rate is  $1160.0879$  kg/s at  $LWC=39$  g/m<sup>3</sup> rain rate. Because distance of each particle is 7 cm, the injection particle number is about 122700.

Before starting to simulate the BWB case, we have to confirm how reliable our CFD tool is. For this reason we choose the ONERA M6 wing as the benchmark case. ONERA M6 wing is a swept wing with symmetrical airfoil and has no twist; its geometry is showing in Table 1. This validation case is considered to be 0.8395 Mach number and the angle of attack is 3.06 degree. Comparison data consists of pressure coefficients at stations along the wingspan obtained in the experiment performed by Schmitt et al., and the computational work performed by Slater through Wind code.<sup>25</sup> In our simulation the total cells number of the structured grid is 3.32 million, solver scheme is pressure-based segregated SIMPLE method, and S-A turbulence model is applied. Some typical results are the  $Y$  plus value of 13-25 at section  $y/b=0.4$  as shown in Fig. 6, and the pressure coefficients distribution at section  $y/b=0.65$  as shown in Fig. 7, with other sections showing similar resemblance to experiment. Indeed the smoothness and close resemblance to experiment for our pressure distribution (Fluent) is quite encouraging.

#### IV. Results and Discussion

We first examine the clear weather condition, after a detailed inspection of our simulated geometric model of BWB configuration, the best  $L/D$  ratio is found at 2 degree AOA at 0.85 Mach number cruising condition. Then again for take-off and landing conditions at speed  $49.4774$  m/s, the best  $L/D$  ratio is at AOA of 4 degree. Both conditions'  $L/D$  ratio vs. AOA is shown in Fig. 8, the large increase of  $L/D$  ratio during take-off and landing situation is quite remarkable but as expected. Again the maximum optimized  $L/D$  ratio of 17.8 and beyond is the first proof of BWB's efficiency and potential. Generally the parasite drag is composed of pressure and skin friction drag, and during cruise the pressure drag will be larger than viscous drag due to the sensitivity of compressible flow wake at subsonic cruise speed. In Qin's result,<sup>11</sup> the best  $L/D$  ratio is at 3 degree AOA and the total drag is composed of 76.6% pressure drag and 23.4% skin friction drag. On the other hand, in our study the best  $L/D$  is at 2 degree AOA while the total drag is 70.2% pressure drag and 29.8% skin friction drag. The similarity in the two drag percentage is rather acceptable, and can be treated as the other validation of current BWB simulation. The detailed drag vs. AOA for current computation is showing in Fig. 9, and the similarity of the two results is obvious. The rapid increase in  $C_{Dp}$  is mainly due to the variation of wake pressure when cruise at different attitude position.

Also, the pitching moment coefficient at Mach number 0.85 and low speed  $49.4772$  m/s are showing in Figure 10. These pitching moment values all decrease rapidly with AOA, suggesting a significant change in flow features over the BWB configuration as AOA increase. The longitudinal stability is measure of response of the aircraft due to changing pitch angle disturbance. When AOA is increased, the BWB moment coefficient is decreased more rapidly at Mach number 0.85 than at speed of  $49.4774$ m/s, suggesting the more negative value (thus more stable) of stability derivative  $C_{m\alpha}$  during cruising. In this study BWB lateral stability derivatives during taking-off and landing phase are considered, with chosen constant crosswind of 10 m/s, 20 m/s and 30 m/s. AOA is in the range of 0 to 12 degree and four side-slip angles are 0, 11.426, 22.010, and 31.230 degree. To test the efficiency and validity of inviscid Euler solver, we first compute the rolling moment and yawing moment coefficients vs. side-slip angle at AOA 0 degree and 1 degree. As showing in Figs. 11 and 12, both the inviscid and viscous solvers have the same tendency, so Euler solver is suited as design tool. For 0 degree AOA, the BWB is lateral and directional stable for all crosswind conditions. But if AOA is slightly increased; our BWB become unstable if crosswind is encountered. This sensitivity in BWB lateral/directional stability may require further attention in the stability and control loop design.

As would be expected for configuration with high swept planform; the level of lateral stability increases with AOA to higher values. This lateral stability may have an adverse impact on landing operations in crosswind without vertical tails. To further investigate our BWB's static stability situation under crosswind condition, rolling and yawing moment coefficients vs. AOA variation has also been simulated. As shown in Figs. 13-16, both  $C_{l\beta}$  and  $C_{n\beta}$  stability derivative values showing the similar behavior: if AOA is greater than 1 degree and crosswind speed is larger than 10 m/s, these derivatives become unstable. The reason is as AOA increase, one of the trailing vortices near the winglets tends to burst over the wing due to crosswind, this effect is enhanced for BWB because now there is no obstacle of cross flow, which may reduce lateral stability even further. Again this is quite contrary to the ordinary civil transport aircraft's stability situation, and partially explains why BWB transport has not been built earlier.

Also, two different rain rates are employed for investigating the heavy rain effects to BWB. During taking-off or landing the BWB has a speed of  $49.4772$  m/s, with  $LWC$  of  $25$  g/m<sup>3</sup> and  $39$  g/m<sup>3</sup>. The success of the DPM module via two-phase flow approach for the heavy rain influence can lead us to analyze the drag distribution details for this BWB. Table 2 shows the pressure and viscous skin friction drag data at 4 degree AOA (best  $L/D$ ) and different rain

rates. This drag distribution percentage ratio is different from Fig. 9 due to the difference in flight speed and attitude. It is observed that at  $25 \text{ g/m}^3$  rain rate, both drag components increase as expected but at roughly the same pace; while as rain rate increase to  $39 \text{ g/m}^3$ , pressure drag increase faster than the viscous skin friction drag, representing that the velocity and thus pressure distribution may have larger variation than the water film boundary layer change for BWB under most severe rainfall. This nonlinear increase in drag may due to heavy rain effect coupled with the peculiar BWB shape.

Further detailed results of lift, drag, and L/D ratio for our BWB under two heavy rain rates are showing in Table 3 and Figs. 17-20. While the LWC of  $39 \text{ g/m}^3$  has stronger degradation impact than the  $25 \text{ g/m}^3$  case as expected, the lift and drag variation under the rain effects are quite different. The heavy rain will pilot the maximum lift coefficient reduction at small AOA and gradually diminish its effect as AOA increase, but the maximum increase of drag coefficient will happen at AOA about 6 degree. Thus the maximum L/D ratio degradation exists in the AOA range of 0 to 6 degree, with slightly variation in that range. Since all civil transport is take-off/landing in that AOA range, this 10 to 15% L/D ratio reduction due to heavy rain represents an important finding for our BWB. Also, it is interesting to notice that under all circumstances the maximum L/D ratio still at 4 degree AOA.

## V. Conclusion

In this study, after gaining confidence in our simulation by testing the M6 wing case, we have completed the full BWB simulation and achieved the best L/D ratio of 17.808 at 2 degree AOA with 0.85 Mach number cruise speed. Also the taking-off and landing condition was simulated with the best L/D is 23.9269 at 4 degree AOA. As for the severe weather effects, our apprehension is concentrated in the low speed take-off/landing case, and three different side-slip angle change due to crosswinds and two different heavy rain rates are fully investigated. According to our simulation, this BWB configuration shows very different stability behavior than conventional transport aircraft. Table 4 shows the comparison of Boeing 747-100, a typical civil transport, and our BWB static stability data. The BWB stability derivative values are differ from B747-100 either in sign or in magnitudes, representing the intrinsic nature of BWB statically unstable tendency. Also, through the DPM module of the two-phase flow approach of the Fluent code, we can successfully simulate most of the heavy rain effect on wing surface such as impingement of rain droplets, water film build, change in lift, drag, pitching moment, and even the pressure and skin friction drag distributions. But fail to detect the detailed heavy rain behavior such as water layer surface waves, rivulet or bead build up, and transition to turbulence. The heavy rain influence is that the lift decrease and drag increase at all angle of attack spectra, and liquid water content of  $39 \text{ g/m}^3$  is more detrimental than  $25 \text{ g/m}^3$ , with maximum lift reduction is at 0 degree and maximum drag increase is at 6 degree AOA. It is observed that although heavy rain will not induce large variation in stall angle of attack, but the degradation in maximum L/D ratio could reach a stunning 10 to 15 percent at low AOA attitude. Finally, we verify that the BWB aerodynamic efficiency degradation under severe weather is worst than expected; and the numerical simulation of BWB under crosswinds and heavy rain will always play important roles for civil aircraft company to design the next generation transport aircraft.

## Acknowledgments

The support of this work by the National Science Council, ROC, under the contract NSC 98-2221-E-032-027 is gratefully acknowledged.

## References

- <sup>1</sup>Wan, T. and Wu, S. W., "Aerodynamic Performance Analysis under the Influence of Heavy Rain," *Journal of Aeronautics, Astronautics and Aviation*, Vol. 41, No. 3, 2009, pp. 173-180.
- <sup>2</sup>Fluent's User Guide.
- <sup>3</sup><http://www.flightglobal.com>.
- <sup>4</sup>Northrop, J. K., "The Development of All-Wing Aircraft," *Journal of Royal Aeronautical Society*, Vol. 51, 1947, pp. 481-510.
- <sup>5</sup>[http://www.aircraftinformation.info/gallery\\_bombers\\_cancelled.htm](http://www.aircraftinformation.info/gallery_bombers_cancelled.htm).
- <sup>6</sup><http://www.aviationexplorer.com>.
- <sup>7</sup>Liebeck, R. H., Page, M. A. and Rawdon, B. K., "Blended Wing Body Subsonic Commercial Transport," *AIAA Paper 98-0438*, 1998.
- <sup>8</sup>Leifur, T. L. and Mason, W. H., "The Blended Wing Body Aircraft," Virginia Polytechnic Institute and State University, Blacksburg, 2006.
- <sup>9</sup>Qin, N., Vavalle, A., Moigne, A. L., Laban, M., Hockett, K., and Weinerfelt, P., "Aerodynamic Studies of Blended Wing Body Aircraft," *AIAA Paper 2002-5448*, 2002.

<sup>10</sup>Roman, D., Gilmore, R., and Wakayama, S., "Aerodynamics of High-subsonic Blended Wing Body Configuration," *AIAA Paper 2003-554*, 2003.

<sup>11</sup>Qin, N., Vavalle, A., Moigne, A. L., Laban, M., Hockett, K., and Weinerfelt, P., "Aerodynamic Considerations of Blended Wing Body Aircraft," *Progress in Aerospace Sciences*, Vol. 40, 2004, pp. 321-343.

<sup>12</sup>Wan, T. and Yang H., "Aerodynamic Performance Investigation of a Modern Blended-Wing-Body Aircraft under the Influence of Heavy Rain Condition," *Proceedings of the 27th International Congress of Aeronautical Sciences (ICAS)*, Nice, France, September 19-24, 2010.

<sup>13</sup>Fremaux, C. M., and Hall, R. M., "Computational Methods for Stability and Control," NASA CP-2004-213028 PT1, April 2004.

<sup>14</sup>Nelson, R. C.: *Flight Stability and Automatic Control*, 2nd edition, McGraw-Hill, N.Y., 1998.

<sup>15</sup>Pao, S. P., Biedron, R. T., Park, M. A., Fremaux, C. M., and Vicroy, D. D., "Navier-Stokes Computations of Longitudinal Forces and Moments for a Blended Wing Body," *AIAA 2005-0045*, 2005.

<sup>16</sup>Rhode, R. V., "Some Effects of Rainfall on Flight of Airplanes and on Instrument Indications," NACA TN 903, April 1941.

<sup>17</sup>Markowitz, A. M., "Raindrop Size Distribution Expression," *Journal of Applied Meteorology*, Vol. 15, 1976, pp.1029-1031

<sup>18</sup>Luers, J. and Haines, P., "Heavy Rain Influence of Airplane Accidents," *Journal of Aircraft*, Vol. 20, No. 2, Feb 1983.

<sup>19</sup>Bilanin, A. J., "Scaling Laws for Testing Airfoils under Heavy Rainfall," *Journal of Aircraft*, Vol. 24, No. 1, Jan. 1987, pp. 31-37.

<sup>20</sup>Bezoz, G. M. and Campbell, B. A., "Development of a Large-Scale, Outdoor, Ground-Based Test Capability for Evaluating the Effect of Rain on Airfoil Lift," NASA TM-4420, April 1993.

<sup>21</sup>Valentine, J. R. and Decker, R. A., "Tracking of Raindrops in Flow over an Airfoil," *Journal of Aircraft*, Vol. 32, No. 1, Jan-Feb.1995, pp. 100-105.

<sup>22</sup>Thompson, B. E., Jang, J., and Dion, J. L., "Wing Performance in Moderate Rain," *Journal of Aircraft*, Vol. 32, No. 5, Sept.-Oct. 1995, pp. 1034-1039.

<sup>23</sup>Wan, T. and Pan, S. P., "Aerodynamic Efficiency Study under the Influence of Heavy Rain via Two-Phase Flow Approach," *Proceedings of the 27th International Congress of Aeronautical Sciences (ICAS)*, Nice, France, September 19-24, 2010.

<sup>24</sup>Bardina, J. E., Huang, P. G., and Coakley, T. J., "Turbulence Modeling Validation, Testing, and Development," NASA Technical Memorandum 1997.

<sup>25</sup>The ONERA M6 Wing, available on-line; URL:<http://www.grc.nasa.gov/www/wind/valid/m6wing/m6wing01/m6wing01.html>

Table 1 ONERA M6 wing geometry.<sup>25</sup>

Mean Aerodynamic Chord	0.64607 meters
Aspect Ratio	3.8
Taper Ratio	0.562
Leading-edge Sweep	30.0 degrees
Trailing-edge Sweep	15.8 degrees

Table 2 BWB drag coefficient with heavy rain at AOA=4 degree

Liquid water content	Pressure drag coefficient	Viscous drag coefficient	Total drag coefficient
0 g/m <sup>3</sup>	0.006151	0.0047995	0.010951
25 g/m <sup>3</sup>	0.006397	0.0048521	0.011250
39 g/m <sup>3</sup>	0.007002	0.0049257	0.011928

Table 3 The C<sub>L</sub> decrease and C<sub>D</sub> increase percentage variation with liquid water content of 25 g/m<sup>3</sup> and 39 g/m<sup>3</sup>

$\alpha$ (deg)	C <sub>L</sub> decrease (LWC= 25g/m <sup>3</sup> )	C <sub>L</sub> decrease (LWC= 39g/m <sup>3</sup> )	C <sub>D</sub> increase (LWC= 25g/m <sup>3</sup> )	C <sub>D</sub> increase (LWC= 39g/m <sup>3</sup> )

0	7.840	11.831	2.376	4.8650
1	5.952	8.669	1.879	3.718
2	2.940	5.198	2.686	5.850
3	3.262	6.328	2.126	3.742
4	1.802	3.144	2.740	8.932
6	1.324	1.909	5.204	11.150
8	0.680	1.561	2.770	4.628
10	0.779	1.139	2.428	4.110
12	0.625	0.929	1.168	2.530

Table 4 Boeing 747-100 and Blended-Wing-Body stability data

Type	C <sub>m<math>\alpha</math></sub> <sup>1</sup>	C <sub>m<math>\alpha</math></sub> <sup>2</sup>	C <sub>l<math>\beta</math></sub> <sup>2</sup>	C <sub>n<math>\beta</math></sub> <sup>2</sup>
B747-100	-1.6	-1.45	-0.281	0.184
BWB	-0.02892-	0.012625	6.068E-4	-2.063E-4

Note: superscript 1 is cruise condition, 2 is landing condition

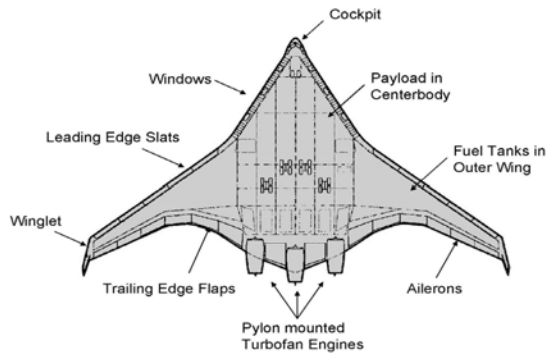


Figure 1. The Boeing BWB baseline.<sup>7</sup>

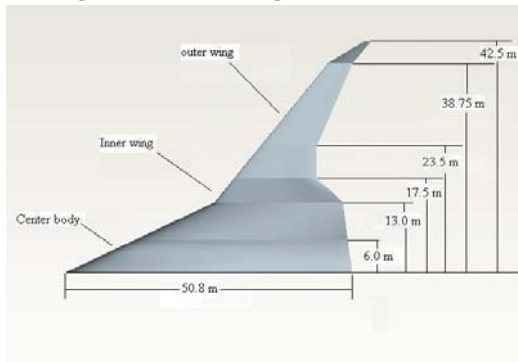


Figure 2. Blended Wing Body geometry model.<sup>12</sup>

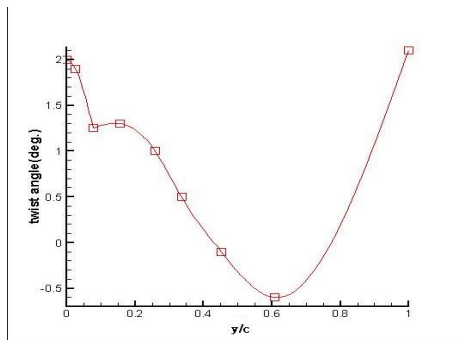


Figure 3. Twist angle distribution.

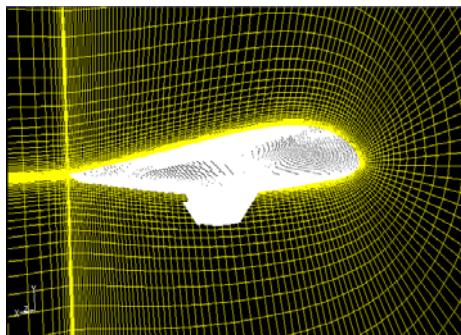


Figure 4. Near mesh of the Blended Wing Body.

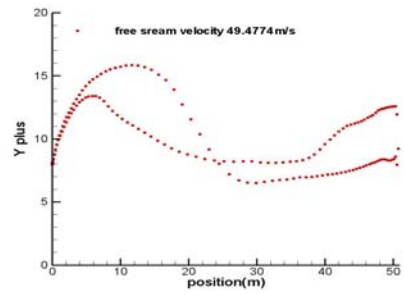


Figure 5. The Y plus distribution with free stream velocity 49.4774 m/s.

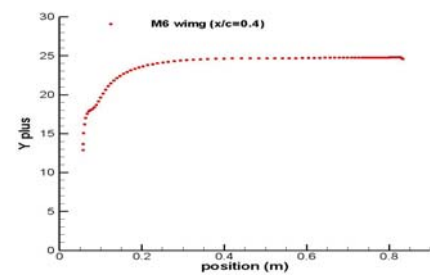


Figure 6. The Y plus of M6 wing at  $y/b=0.4$ .

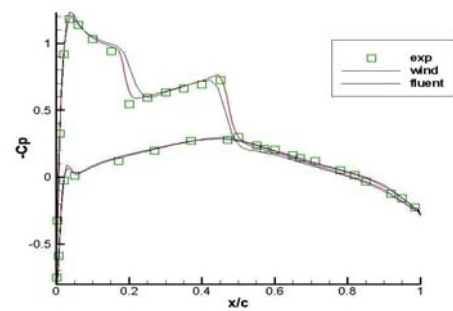


Figure 7. M6  $C_p$  distribution at section  $y/b=0.65$ .

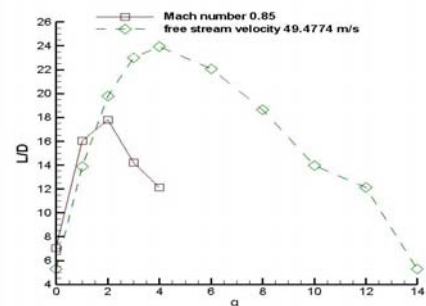


Figure 8. BWB lift to drag ratio vs. AOA at two different speeds.

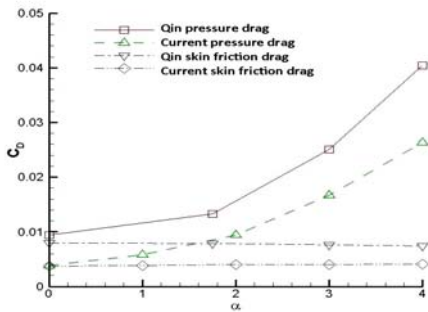


Figure 9. Pressure drag and skin friction drag comparison.

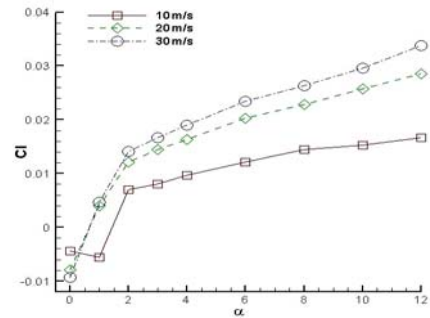


Figure 13. The rolling moment coefficient  $C_l$  vs. AOA at three different crosswinds.

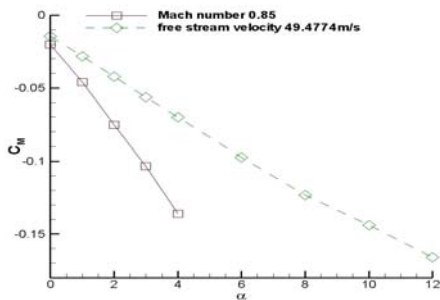


Figure 10. The pitching moment coefficient  $C_M$  vs. AOA at two different velocities.

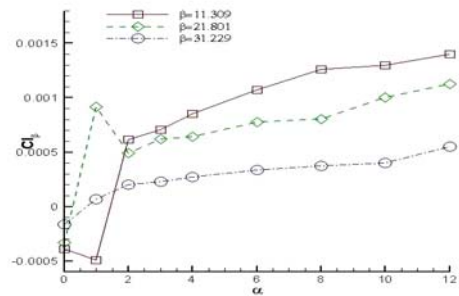


Figure 14. The stability derivative  $C_{l_\beta}$  vs. AOA at three different  $\beta$ .

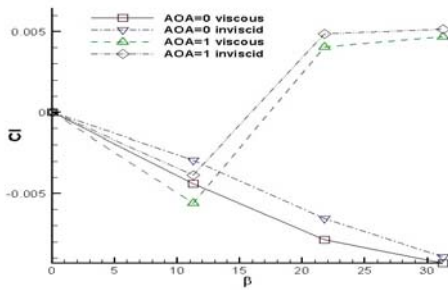


Figure 11. The rolling moment coefficient  $C_l$  vs.  $\beta$  at two different AOA.

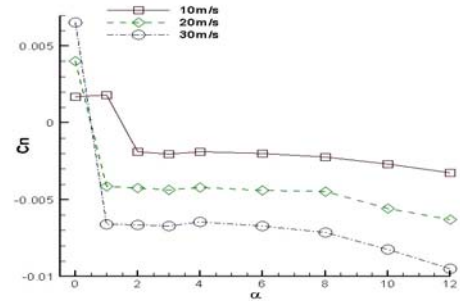


Figure 15. The yawing moment coefficient  $C_n$  vs. AOA at three different crosswinds.

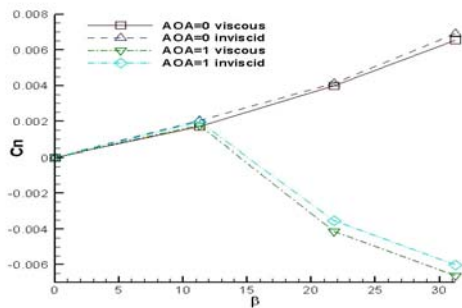


Figure 12. The yawing moment coefficient  $C_n$  vs.  $\beta$  at two different AOA.

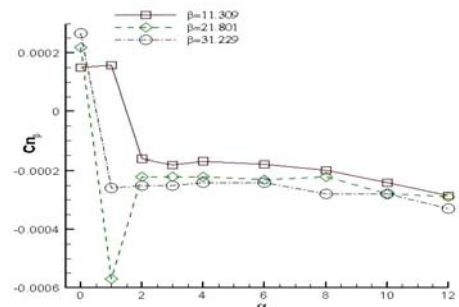


Figure 16. The stability derivative  $C_{n_\beta}$  vs. AOA at three different  $\beta$ .

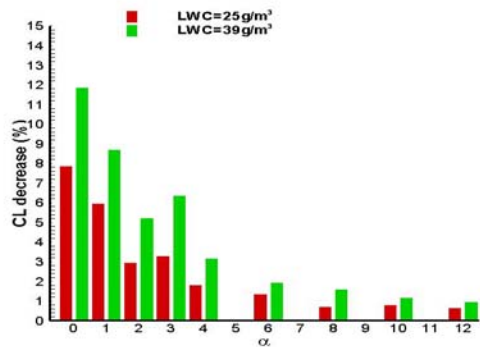


Figure 17. The lift coefficient decrease ratio at two different rain rates.

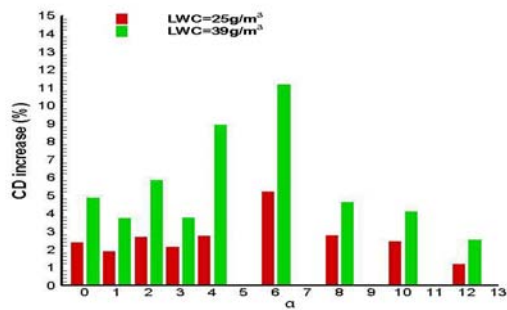


Figure 18. The drag coefficient increase ratio at two different rain rates.

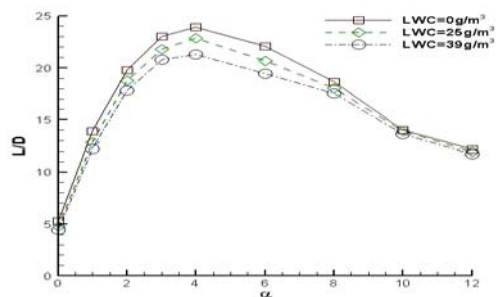


Figure 19. The lift to drag ratio vs. AOA at different rain rates.

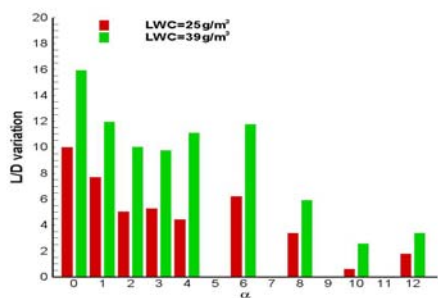


Figure 20. The lift to drag ratio vs. AOA comparison at two rain rates.